

RESEARCH

Open Access



Experimental study on airfoil flow separation control via an air-supplement plasma synthetic jet

Ru-Bing Liu^{1,2*} , Wen-Tao Wei^{1,3}, Hai-Peng Wan¹, Qi Lin^{1,2}, Fei Li⁴ and Kun Tang^{5,6}

*Correspondence:
lrb@xmu.edu.cn

¹ School of Aerospace Engineering, Xiamen University, Xiamen 361102, China

² Fujian Provincial Key Laboratory of Plasma and Magnetic Resonance, Xiamen 361005, China

³ Chengdu Aircraft Design and Research Institute, Chengdu 610041, China

⁴ Shanghai Aerospace Control Technology Institute, Shanghai 201100, China

⁵ Rotor Aerodynamics Key Laboratory, China Aerodynamics Research and Development Center, Mianyang 621000, China

⁶ Science and Technology on Plasma Dynamics Laboratory, Air Force Engineering University, Xi'an 710038, China

Abstract

An air-supplement plasma synthetic jet (PSJ) actuator increases the air supplemental volume in the recovery stage and improves the jet energy by attaching a check valve to the chamber of a conventional actuator. To explore the flow control effect and mechanism of the air-supplement actuator, via particle image velocimetry experiments in a low-speed wind tunnel, the flow field and boundary layer characteristics of a two-dimensional airfoil surface under different actuation states were compared for different attack angles and jet orifices. The experimental results show that, compared with the conventional actuation state, the jet energy of the air-supplement PSJ is higher and the indirect mixing effect of the counter-vortex sequence produced by the jet-mainstream interaction is stronger. Furthermore, the boundary layer mixing effect is better, which can further suppress flow separation and improve the critical flow separation attack angle. Moreover, increasing the jet momentum coefficient can enhance the flow control effect. The findings of this study could provide guidance for the flow control application of air-supplement PSJs.

Keywords: Plasma synthetic jet, Check valve, Flow separation, Active flow control, Air-supplement

1 Introduction

The plasma synthetic jet (PSJ) concept, which was first proposed by Grossman et al. [1] at Johns Hopkins University Applied Physics Laboratory in 2003, is based on spark discharge and has gained increased attention in the field of plasma flow control technology. As this approach exhibits the unique ability of producing high-velocity pulsed jets without additional gas sources, it is particularly tailored for high-speed active flow control in aerospace engineering.

The structure and working process of a PSJ actuator are shown in Fig. 1. The PSJ actuator is composed of a cavity with a hole and a pair of electrodes. Its working process can be divided into three stages: energy deposition, jet ejection, and recovery [2]. The spark discharge generates a large amount of heat, and the air in the chamber suddenly expands upon heating. The high-pressure air emerges from the orifice forming a high-speed jet; then, the external gas is refilled through the jet to prepare for the next discharge. Thus,

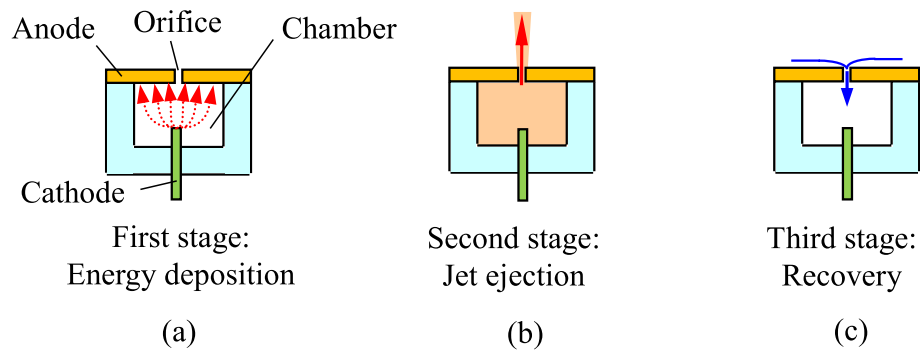


Fig. 1 Working process of a PSJ actuator [2]. Reprinted with permission from the American Institute of Aeronautics and Astronautics, Inc.

the PSJ actuator can generate a high-speed jet in a short time. Moreover, it has a faster speed and higher actuation frequency than piezoelectric and mechanical synthetic jets.

Recently, previous studies on PSJs have made some important progress. In particular, Popkin et al. [3, 4] studied the influence of the actuator structure and actuation mode on jet characteristics to improve the jet performance and experimentally estimated the jet energy efficiency. Zong et al. [5, 6] also studied the energy efficiency characteristics of actuators. Belinger [7] and Wu et al. [8] used different technical approaches to explore the effects of different electrical parameters on jet performance.

To explore the PSJ control effect and mechanism under low-speed flow, Caruana et al. [9] experimentally verified the PSJ control effect on flow separation at the trailing edge of a two-dimensional (2D) airfoil. Twenty PSJ actuators were arranged at $0.32c$ (c : chord length) from the leading edge of a NACA0015 airfoil. The results showed that the drag decreased by 13% at a wind speed of 20 m/s ($Re_c = 6.7 \times 10^5$). Subsequently, Liu et al. [10] arranged two PSJ actuators at $0.15c$ from the leading edge to actively control the flow separation of a NACA0021 airfoil model. The drag coefficient decreased by 33.1%, and the lift-drag ratio increased by 104.2% at a wind speed of 20 m/s ($Re_c = 3.6 \times 10^5$). Li et al. [11] arranged three PSJ actuators at the leading edge of the airfoil to control the flow separation of a high-lift airfoil and found that the airfoil stall angle and maximum lift coefficient increased by 5° and 8.1%, respectively, when the wind speed was 20 m/s. Su et al. [12] designed a new type of multi-channel discharge PSJ and found that a 12-channel PSJ could effectively inhibit the flow separation of the airfoil suction surface, increase lift, and delay stall. At a moderate Reynolds number ($Re_c = 1.7 \times 10^5$), Zong et al. [13] used 26 PSJ actuators arranged at $0.25c$ from the leading edge of a NACA0015 wing model for flow separation control. The maximum stall angle was delayed from 15.5° to approximately 22° , and the maximum lift coefficient was increased by 21%. It was found that the flow separation control mechanism by the PSJs is related to the relative actuation position and the dimensionless actuation frequency. Gu et al. [14] performed a numerical study on active PSJ flow separation control for the rear body of a transporter. Their results showed that the delayed flow separation mechanism by the PSJs is that the jet inputs high-energy momentum into the separation area and the vortex formed via the interaction with the external flow strengthens the external flow mixing with the low-speed boundary layer. Sun et al. [15] used multi-channel PSJs for flow separation control for a flying wing model with three-dimensional flow characteristics at a wind speed of

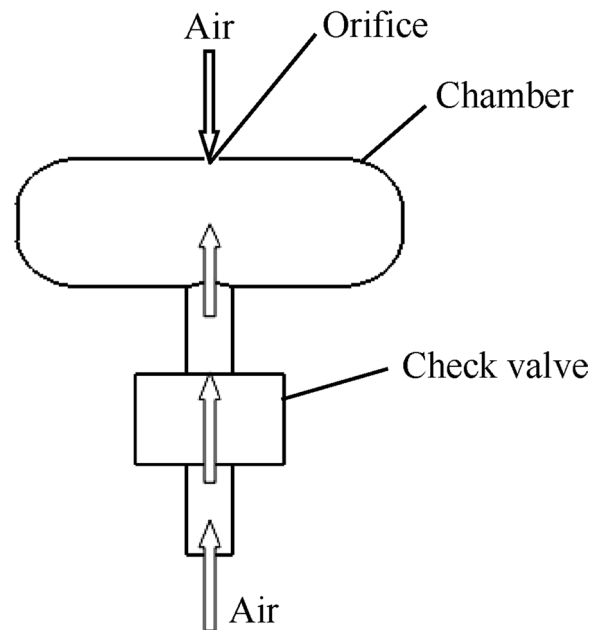


Fig. 2 Schematic of air supplement through a check valve [22]

30 m/s ($Re_c = 9.9 \times 10^5$). They found that the PSJs could significantly enhance the lateral stability of the flying wing model while increasing the lift and decreasing the drag, and the fluctuation range of the rolling moment coefficient was reduced by 66.7%. Zhou et al. [16, 17] also achieved a good flow control effect in supersonic flow by using a three-electrode PSJ actuator.

Although PSJ actuators have many advantages, they rely on the jet hole for suction when the jet is sprayed out, resulting in a limited amount of backfill gas per unit time. In continuous discharge or high-frequency discharge cases, insufficient air supply in the chamber decreases the jet velocity and weakens the flow control effect. To address this problem, Luo et al. [18] proposed a method for realizing the rapid supplement and pressurization of the air in the chamber by using high-speed flow dynamic pressure in a rarefied atmospheric environment. Li et al. [19] designed a new type of actuator configuration using a piezoelectric vibrator to regulate the chamber volume to improve the suction recovery ability. Emerick [20] and Zhou et al. [21] used an external high-pressure gas source to supply air to the discharge chamber of the actuator to significantly improve the jet performance. We previously proposed an air-supplement PSJ actuator [22] that does not need a high-pressure gas source or incoming flow pressure for air supply; instead, it uses a check valve to improve the plasma jet performance (Fig. 2).

The air-supplement spark discharge plasma jet generator connects a check valve to the opposite wall of the discharge chamber jet outlet, as shown in Fig. 2. When the gas in the cavity discharges, a large amount of heat is released by the plasma, which instantaneously expands the gas to form a high-speed jet. Then, in the recovery process, the check valve is automatically opened and closed under a pressure difference inside and outside the cavity, respectively. Under negative pressure in the cavity, the check valve automatically opens to suction the outside air to supplement the gas in the cavity to restore pressure. Under high pressure in the cavity, the check valve automatically closes to prevent

leakage. To restore the air pressure in the cavity after discharge as soon as possible, the channel area at the connection between the check valve and the cavity is set to several times that at the jet orifice, so as to shorten the recovery process and improve the PSJ actuator working frequency [22]. In addition, the proposed actuator can increase the air supply area through the check valve to quickly recover the low pressure in the chamber after the jet ejection, improve the actuator response speed, and increase the jet energy. This actuator has a simple structure, strong working stability, and adaptability. Without external atmospheric environmental influence, it can work in both atmospheric pressure and rare environments. Previous studies on air-supplement PSJs have focused on basic actuator characteristics alone, and there is still a lack of experimental research on flow control applications. Moreover, the flow control effect and mechanism of the air-supplement PSJ actuator are not yet clear.

Therefore, based on the air-supplement actuator, we used the NACA0021 airfoil as the control object in the present study. The actuator was arranged $0.2c$ away from the leading edge of the airfoil. Then, the flow field of the suction surface under three states (i.e., non-actuation, conventional actuation, and air-supplement actuation) at different attack angles was measured through a wind tunnel experiment and particle image velocimetry (PIV) system. The flow field boundary layer characteristic parameters are compared in detail to explore the air-supplement PSJ mechanism and effect on flow separation on a 2D airfoil suction surface. The research results verify the flow control effect of air-supplement PSJ and provide valuable reference information for its practical application. After clarifying the flow control mechanism, these findings could also guide the further optimization of the air-supplement PSJ actuator and improve its control effect.

The remainder of this paper is organized as follows. The experimental setup is described in Section 2. The flow field under different actuation states and PSJ-based flow control mechanism are presented in Sections 3 and 4, respectively. Finally, the results are discussed and the conclusions are drawn in Sections 5 and 6, respectively.

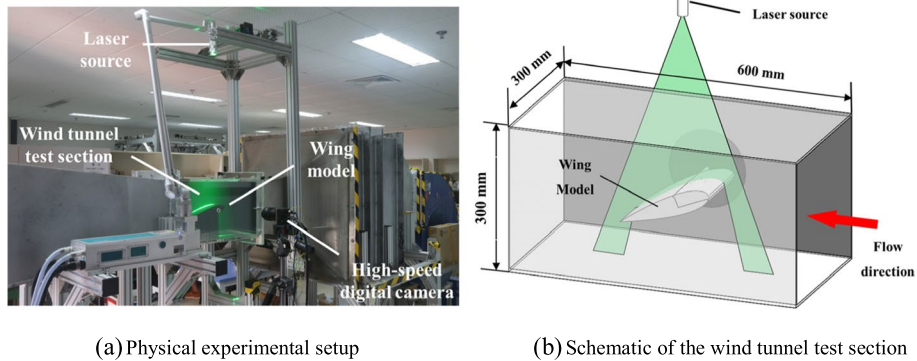
2 Experimental system

To explore the air-supplement PSJ actuator mechanism and effect on airfoil flow separation, PIV was used to photograph the flow field of the NACA0021 airfoil model under different control conditions in a low-speed direct wind tunnel. The experimental system consisted of a low-speed direct wind tunnel, a PIV system, an air-supplement PSJ actuator, and a 2D airfoil model, as shown in Fig. 3.

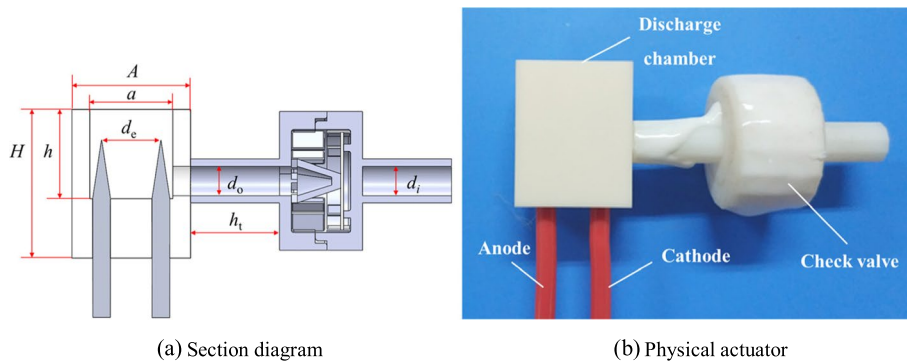
2.1 Low-speed direct wind tunnel and PIV system

A low-speed straight through-type wind tunnel was used in the experiment. As shown in Fig. 3, the experimental cross-section size was 300×300 mm, the experimental section length was 600 mm, and the turbulence level was $\leq 0.5\%$.

The PIV system (SM3-4M200, MicroVec) used in this experiment included a dual-pulse Nd:YAG laser with a 532-nm green light (pulse frequency up to 15 Hz), a high-speed digital camera (SM-CCDB4M20, 2048×2048 resolution), a synchronization controller, a workstation, and control software. The maximum PIV frequency was 15 Hz, and a frequency of 5 Hz was used in this study. The average velocity field was obtained by averaging 100 pairs of images each time. Tracer particles were produced by heating the



(a) Physical experimental setup
Fig. 3 Wind tunnel experimental system



(a) Section diagram
Fig. 4 Structural schematic of the air-supplement PSJ actuator

glycerol on a stage smoker (AB-1500, Svnscomg). To fully reflect the PSJ control effect on the flow field, the PIV test cross-section was located at the spanwise center section of the wing model, which is the center of the jet orifice under a single jet control state.

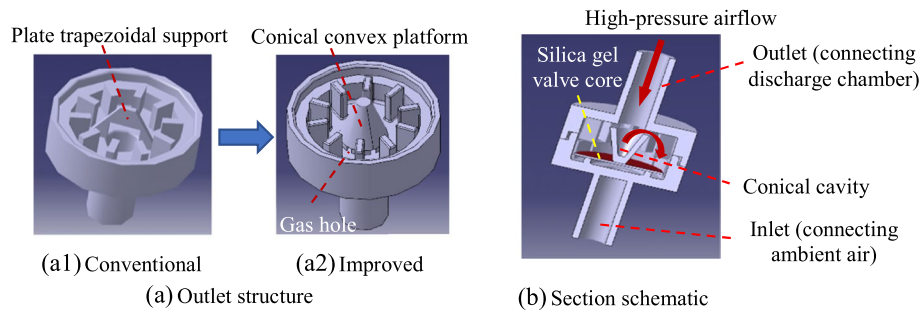
2.2 Air-supplement PSJ actuator and high-voltage pulse power supply system

The air-supplement PSJ actuator used in the experiment consisted of a discharge chamber, a cathode, an anode, and an air-supplement check valve, as shown in Fig. 4. The discharge chamber was fixed inside the wing model using a sealed silica gel to form a closed chamber. Small jet holes were placed at appropriate positions in the airfoil. Two electrode holes were present at the bottom of the discharge chamber, and the cathode and anode were inserted from above the holes. The cathode and anode were connected to the output end of the programmable four-channel high-voltage pulse power supply (XMU-PTLA-DY-02). The side end of the discharge chamber was connected with a check valve.

The actuator chamber was composed of zirconia ceramics with a volume of 1050 mm³. Table 1 lists the model structural parameters. The output voltage amplitude of each programmable four-channel high-voltage pulse power supply channel was approximately

Table 1 Structural parameters of the air-supplement PSJ actuator

Parameter	Value/mm
Actuator length A	20
Discharge chamber length a	14
Actuator width B	10
Discharge chamber width b	5
Actuator height H	25
Discharge chamber height h	15
Electrode spacing d_e	10
Length of check valve outlet h_t	15
Diameter of check valve inlet d_i	4
Diameter of check valve outlet d_o	4

**Fig. 5** Check valve structure [24]

0–20 kV, the frequency was approximately 20 Hz–5 kHz, and the duty cycle was approximately 5%–50%. The anode and cathode were composed of silica gel wire.

The check valve is a specially designed plastic diaphragm check valve. It is mainly composed of an inlet port, a valve core, and an outlet port. As the actuator working frequency was as high as hundreds of Hertz, the response speed of the silica gel valve core of an ordinary check valve could not provide the refilling frequency required by the experiment. The high-frequency and high-pressure reverse airflow inside the actuator directly affected the check valve core, leading to deformation and leakage and causing the actuator jet velocity to decrease.

To weaken the reverse impact of internal high-pressure airflow on the valve core, the check valve structure was specially designed. The support structure of the valve core in the outlet end was changed from a plate trapezoidal support (Fig. 5a1) to a conical convex platform (Fig. 5a2). Gas holes were opened at the bottom of the convex platform for gas inlet and outlet [23]. While supporting the valve core, the conical convex platform had a buffer effect on the reverse flow, which effectively improved the reverse opening pressure. When the check valve worked, the high-pressure airflow in the actuator cavity entered the one-way valve. The reverse airflow that directly affected the valve core first entered the conical cavity and acted on the inner wall of the conical cavity. After the airflow was buffered, it entered the one-way valve cavity through the gas hole at the bottom of the conical convex platform, effectively avoiding the direct impact of the high-pressure airflow on the valve core, as shown in Fig. 5b [24].

The check valve was produced via 3D printing using a high-temperature-resistant resin. Through previous experiments, it was found that the check valve had the best air supply effect when the silica gel valve core thickness was 0.3 mm, so a valve core with this thickness was used for subsequent research.

2.3 NACA0021 2D wing model

A NACA0021 airfoil with a relatively large thickness was selected to design the 2D wing model and facilitate the installation of air-supplement PSJ actuators. The main body of the model was composed of ABS plastic, the chord length c was 200 mm and the span length l was 250 mm, as shown in Fig. 6.

The upper wing of the model had an actuator jet outlet, and the air-supplement PSJ actuator was installed inside the model, as shown in Fig. 6a. The installation position of the jet outlet was determined based on the flow separation point position. Amitay et al. [25] and Zong et al. [13] demonstrated that the jet near the separation point has the best control effect. At low speeds, the flow separation point of the NACA0021 airfoil was concentrated near $x/c=0.2$, where x is the distance from the airfoil surface position projection on the chord length to the leading edge. Therefore, the jet outlet was arranged at $x/c=0.2$ to achieve a better flow control effect. The jet outlet was perpendicular to the airfoil surface and was located in the spanwise center. It had an aperture of 1.2 mm, and the model thickness was 3 mm. The actuator was mounted on the wing surface with sealed silica gel, and the discharge chamber was facing the jet hole. The fixed rod could be installed in the model to fix it in the wind tunnel test section.

In this experiment, due to wind tunnel test condition and airfoil model size limitations, on the one hand, the aerodynamic force measurement experiment cannot be carried out. On the other hand, the internal space of the model is limited, as is the number of actuators that can be arranged. Accordingly, only one actuator is arranged to carry out the experiment. However, the jet control effect has a certain range in the spanwise direction. Previous research [26, 27] also showed that the action range of the jet could reach more than 10 times the distance range of the jet orifice. Therefore, the flow field near the excitation position of the jet hole is measured via PIV to explore the control effect of the jet.

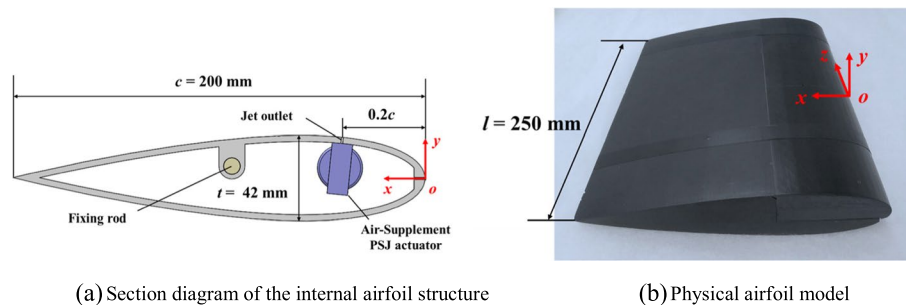


Fig. 6 Schematic of the 2D airfoil model

3 Flow separation control effect of the air-supplement PSJ actuator at different attack angles

To explore the air-supplement PSJ flow separation control effect, PIV technology was used to measure the flow field on the upper wing before and after the flow separation critical attack angle in the wing model under different actuation conditions. According to the flow field, the changes in the flow separation critical attack angle α^* , backflow area $S_{U<0}$ above the airfoil, and relative position s/c of the flow separation point on the airfoil (s is the distance from the flow separation point projection on the chord length to the leading edge) under different actuation conditions were compared and analyzed. The different incentive states included non-actuation, conventional actuation, and air-supplement actuation with three control states; the non-actuation state was the reference state when the actuator was closed. In the conventional actuation state, when the actuator was working, the inlet end of the check valve was sealed with sealed silica gel to cut off the air supply. In the air-supplement actuation state, the check valve inlet was kept open and air was supplied. α^* is the minimum angle for airfoil flow separation, reflecting the difficulty of airfoil flow separation. The greater the angle, the more difficult the flow separation. The critical attack angle variation $\Delta\alpha^*$ under different actuation states can effectively characterize the actuator flow control effect. The velocity recirculation zone is the area in which the transverse velocity component is opposite to the incoming velocity in the flow field profile of the upper wing. $S_{U<0}$ indicates the separation degree of the upper wing flow field. The larger this value, the more intense the flow separation. It can be used to measure the PSJ flow separation control effect. Point location s/c indicates the flow separation location. The larger this value, the farther the flow separation. To some extent, it can also measure the PSJ flow separation control effect.

According to our previous research on the air-supplement PSJ actuator working mechanism [24], there is an effective working frequency range at which the air-supplement actuator works normally. The effective working frequency range of the air-supplement actuator used in this experiment is approximately 160–300 Hz. To ensure the working reliability of the actuator, the experimental parameters were set as follows: loading voltage amplitude $U_a = 15$ kV, actuation signal pulse width $t_p = 1$ ms, and actuation signal frequency $f = 250$ Hz. Moreover, the jet peak velocity V_p and the average velocity V_a were 31.66 and 10.12 m/s, respectively, under air-supplement actuation, and 27.94 and 8.65 m/s, respectively, under conventional actuation.

We installed the actuator at $x/c = 0.2$ inside the wing surface on the wing model. At a wind speed v of 5 m/s and Reynolds number Re of 6.7×10^4 (based on c), the flow field on the airfoil surface under different actuation states was measured to explore the flow separation control effect of jet actuation. The airfoil attack angle α increased from 5° to 12° , and each interval $\Delta\alpha = 1^\circ$ corresponded to a group. A total of 100 flow field image pairs were taken in each state, which were averaged as the flow field results.

3.1 Flow field comparison under different actuation states at different attack angles

The wind tunnel test results show that the airfoil surface flow field state varies under different actuation conditions for the same α . Moreover, the flow separation α^* in the non-actuation, conventional actuation, and air-supplement actuation states is 8° , 10° , and 11° , respectively. Figure 7 shows the flow field velocity contours of the upper wing under the

three actuation states. The velocity $U_c = U/U_\infty$, where U_∞ is the incoming wind speed, in the contour is dimensionless. The solid black line in the contour is the separation streamline to characterize the separated flow region, which starts from the separation point with zero velocity on the airfoil surface. The dotted black line is the zero-velocity line, and the area between the zero-velocity line and the upper surface of the model is the velocity backflow area. In this area, the direction of the transverse velocity component of the flow field velocity is opposite to that of the incoming flow velocity. In Fig. 7, the black arrow represents the velocity vector and the red arrow in the airfoil represents the jet control position.

Air-supplement actuation can improve the flow separation α^* , inhibit flow separation generation on the airfoil wing surface, and improve the control effect compared to that in the conventional actuation state (Fig. 7). Compared with the non-actuation ($\alpha^* = 8^\circ$) and conventional actuation states ($\alpha^* = 10^\circ$), air-supplement actuation ($\alpha^* = 11^\circ$) has a better inhibitory effect on the flow separation of airfoil, and the critical attack angle α^* for flow separation increases by 3° and 1° , respectively, as shown in Fig. 7. The control effect of conventional actuation is similar to the increase in the stall angle of the NACA0021 wing model by a PSJ in a previous study [10]. In addition, it is similar to the control effect of the NACA0021 wing model by a conventional synthetic jet with an injection angle of 90° adopted by Gu et al. [28].

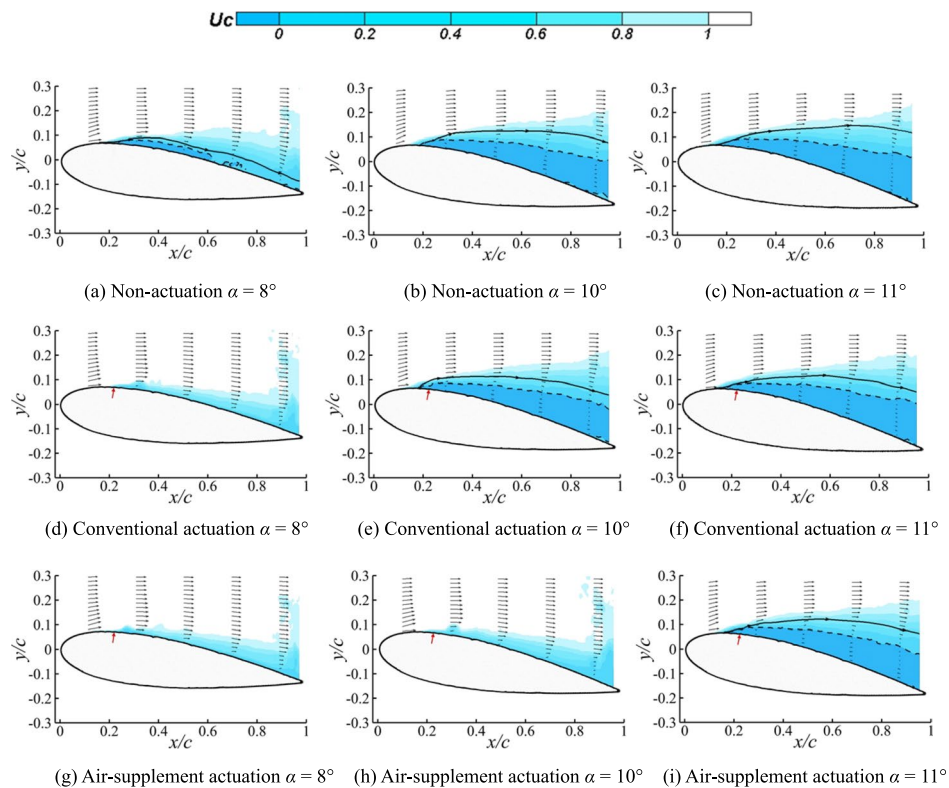


Fig. 7 2D airfoil upper surface velocity contour under different actuation states. Black arrows: velocity profiles at selected streamwise locations; solid black line: separating streamline; dotted black line: contour lines of $U_c = 0$ (referred to as zero-velocity lines); the jet orifice position is indicated by a red arrow

3.2 Flow separation characteristic parameters comparison under different actuation states

In addition to the qualitative observation of the flow field velocity contours on the airfoil surface, the backflow region area and flow separation point position are also important parameters for investigating the degree of flow separation. Therefore, based on the PIV flow field measurement results of the above airfoil surface, we further quantitatively calculated the dimensionless backflow zone area $S_{U<0}/S_0$, where S_0 is the 2D airfoil cross-sectional area, under different actuation states and the relative flow separation point position s/c on the airfoil, as shown in Fig. 8.

Under the three actuation states, after flow separation occurs on the airfoil surface, with increasing α , $S_{U<0}$ increases gradually, and s/c decreases gradually. The separation position moves to the leading edge, and the degree is more intense. Compared with the non-actuation and conventional actuation states, the backflow region area is smaller, and the separation point position is more backward, which has better inhibitory effects on flow separation. Furthermore, compared with the conventional actuation case, the air-supplement actuation inhibitory effect on the backflow area and the delay effect on the separation point position are increased by 102.43% and four times, respectively.

Based on the experimental results, the conventional PSJ can inhibit flow separation and improve the flow separation α^* . However, after separation occurs, the flow control effect is weak. Compared with the conventional jet, the air-supplement PSJ can not only further improve the flow separation α^* , but also the control effect after separation.

After clarifying the flow separation control effect of the air-supplement PSJ actuator, it was necessary to further clarify the flow separation control mechanism with an air-supplement PSJ to provide guidance for flow control optimization. The necessary conditions for flow separation in the boundary layer are the fluid viscous force and the existence of a certain inverse pressure gradient in the flow field. The ability to resist the reverse pressure gradient is what the jet can change under active flow control. The main parameters that reflect this ability are the boundary layer velocity profile and the displacement thickness. The velocity profile is composed of velocity profiles at several positions, which can visually represent the velocity variation along the airfoil chord. The fuller the velocity profile, the stronger the ability of the boundary layer flow to resist the reverse pressure gradient and the PSJ flow control effect. The boundary layer displacement thickness

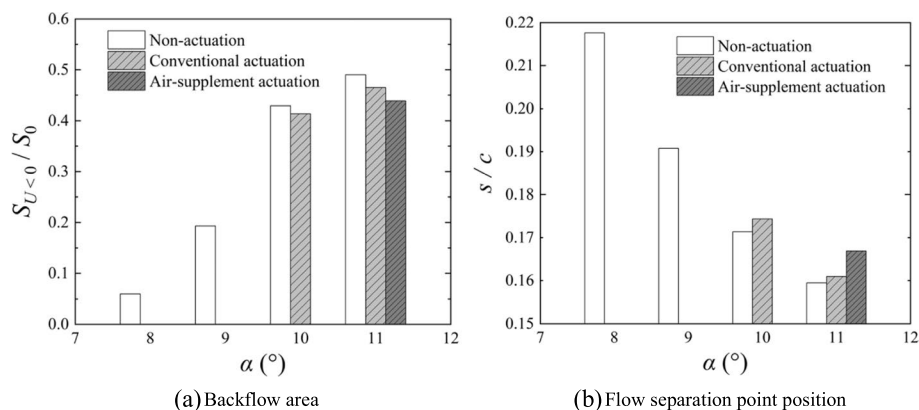


Fig. 8 Flow separation characteristic parameter variation according to the attack angle under different actuation states

δ^* reflects the boundary layer mass loss due to the viscous force (Eq. 1). The smaller δ^* , the less the mass flow loss, and the more significant the flow control effect.

$$\delta^* = \int_{y_0}^{y_r} \left(1 - \frac{U}{U_{max}} \right) dy, \quad (1)$$

where U is the velocity, U_{max} is the peak velocity on the profile, y_0 is the starting position of the velocity profile, and y_r is the position when the velocity reaches U_{max} .

Although the boundary layer velocity profile and δ^* can deepen the understanding of the flow control mechanism; the velocity profile is still a result of jet action. To reveal the flow mechanism, we must study the flow structure generated by the jet (i.e., vortex structure). Gu et al. [28] showed that the control effect of a synthetic jet on airfoil flow is through the vortex structure generated by the jet, increasing the mixing effect between the airflow inside and outside the boundary layer and introducing the outer high-momentum flow into the boundary layer. Moreover, Zong et al. [27] found that the reverse vortex pair generated by a PSJ can significantly enhance the ability of the flow boundary layer to resist the reverse pressure gradient. The vortex structure produced by the jet is the key to clarifying its control flow separation mechanism. Therefore, it is necessary to compare the changes in the vortex structure under different actuation states to reveal the enhancement mechanism of the flow separation control effect under air-supplement actuation.

To explore the flow separation control mechanism with the air-supplement PSJ, we compared the changes in the flow field velocity profile, δ^* , and the vortex structure under different actuation states (non-actuation, conventional actuation and air-supplement actuation) based on the results at $\alpha = 10^\circ$ in Section 3.1 (Fig. 7b, e, and h).

3.3 Velocity distribution and displacement thickness under different actuation states

The measured flow field, as discussed in Section 3.1, is processed to obtain the flow field velocity profiles on the upper wing and the boundary layer displacement thickness. The boundary layer velocity profiles are extracted along the normal direction at an airfoil surface position of $x/c = 0.1 \sim 0.8$ at an interval of $\Delta x/c = 0.1$. Figure 9 shows the velocity profiles of the upper wing under three different excitation conditions at $\alpha = 10^\circ$. The vertical coordinate y is the boundary layer height, which is nondimensionalized by the maximum airfoil thickness t . The horizontal coordinates are $x/c + 0.05 U/U_{max}$, which reflect the position and fullness of the velocity profiles [29].

Compared with the non-actuation and conventional actuation states, the velocity profile at each position of the upper wing flow field under air-supplement excitation is fuller, the flow velocity is greater at the same height, and the ability of the air flow to resist the reverse pressure gradient is stronger. Therefore, the airfoil flow separation α^* is improved, as shown in Fig. 7.

Figure 10 shows the variation in δ^* according to x/c under different excitation conditions at $\alpha = 10^\circ$. The vertical coordinate is the displacement thickness, which is dimensionalized by t . The red arrow indicates where the jet is applied. Compared with the non-actuation and conventional actuation states, the jet can significantly reduce δ^* under air-supplement excitation when $x/c > 0.2$. The influence of the conventional excitation on

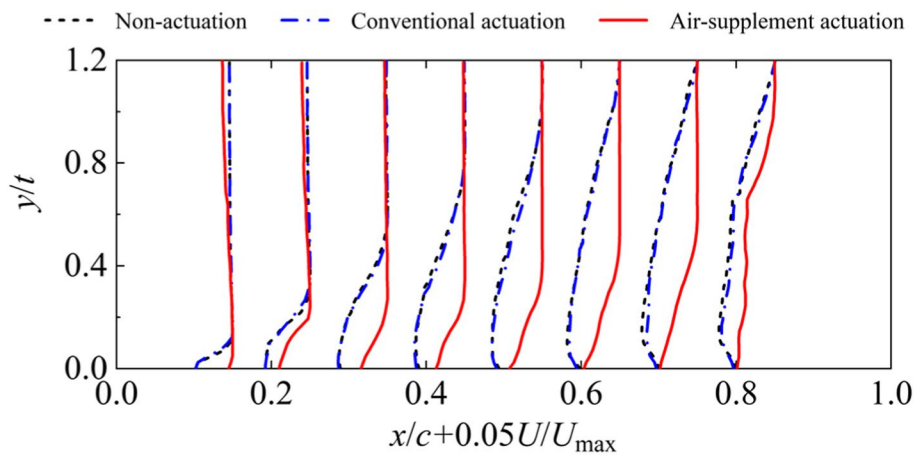


Fig. 9 Velocity profile of the suction surface under different actuation states at $\alpha = 10^\circ$

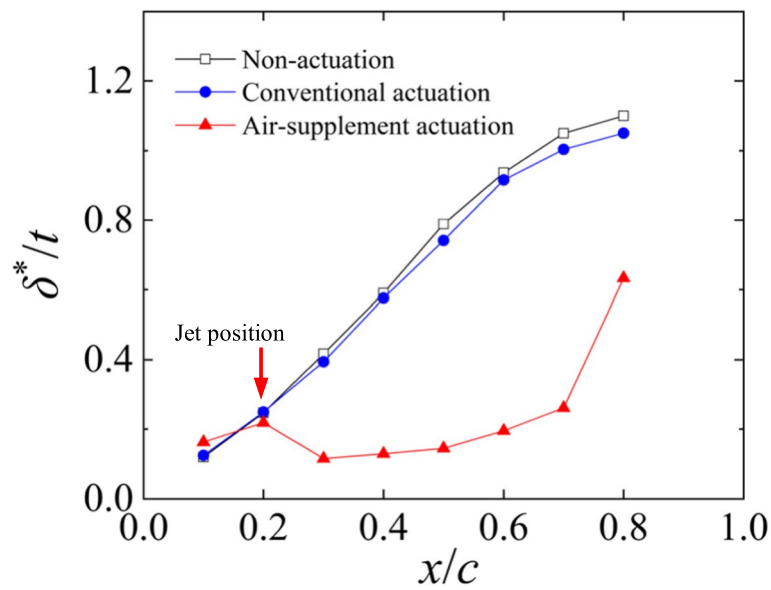


Fig. 10 Boundary layer displacement thickness under different actuation states at $\alpha = 10^\circ$

δ^* is weakened when $\alpha = 10^\circ$. At $x/c = 0.5$, the jet only decreases δ^* by 6.0%. Moreover, under air-supplement excitation, the jet can still reduce δ^* by 81.7%.

3.4 Vortex structure under different excitation conditions

Based on the velocity fields shown in Fig. 7b, e, and h, the flow field vortex contour and streamline diagram on the airfoil upper surface under the three actuation states at $\alpha = 10^\circ$ are shown in Fig. 11. The vortex is identified via the Q criterion.

Under non-actuation (Fig. 11a), flow separation occurs from the leading edge, and the vortex structure appears near the flow separation point, but the scale is small and

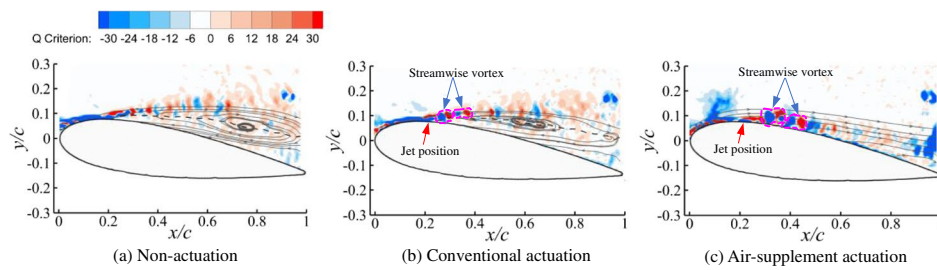


Fig. 11 Vortex contours and streamlines under different actuation states at $\alpha = 10^\circ$

dense. Under the influence of the viscous force and the inverse pressure gradient, there is a large range of velocity backflow in the boundary layer, mixing with the mainstream along the inflow direction, and the small-scale vortex gradually develops into a large-scale irregular vortex structure. Under conventional actuation (Fig. 11b), although the jet cannot inhibit flow separation, it interacts with the mainstream and generates a stream-wise counter-vortex structure at the jet actuation position. The counter-vortex develops downstream with the mainstream and gradually dissipates, evolving into an irregular vortex structure. Under air-supplement actuation (Fig. 11c), the jet energy is higher, and flow separation is completely suppressed. The range of the generated counter-vortex structure is significantly larger than that under conventional excitation, and it is basically attached to the airfoil surface. This indicates that the PSJ flow control effect is noticeably better than that under the conventional and air-supplement actuation states.

4 Effect of jet orifice diameter on the flow separation control effect

As an important structural parameter of a PSJ actuator, the jet orifice diameter affects not only the jet velocity characteristics, but also the jet flow, which is bound to change the jet flow control effect. Therefore, this section focuses on the influence of the jet orifice on the control effect.

4.1 Jet velocity comparison

First, the peak velocity V_p of an air-supplement PSJ with a jet orifice diameter d of 0.8, 1.2, 1.6, and 2.0 mm was measured. The results obtained with a voltage amplitude U_a of 15 kV, pulse width t_p of 1 ms, and frequency f of 250 Hz are shown in Fig. 12.

The velocity measurement results show that under the same electrical parameters, with an increase in d , the jet V_p increases first and then decreases, and the maximum V_p appears at $d = 1.6$ mm. The reason is that when d is small, the viscous force has obvious influence, the throat boundary layer has a blocking effect, and the jet velocity increases as the aperture increases. However, as d further increases to a critical value, the jet mass flow becomes saturated, and reduces the jet velocity [30–32]. The critical d is determined by the discharge energy and the actuator chamber volume. In this experiment, the actuator with $d = 1.6$ mm obtained the maximum jet velocity. For different diameters, the actuator jet velocity under air-supplement actuation is more than 10% higher than that under conventional actuation. This finding shows that the check valve is effective for different jet orifice diameters.

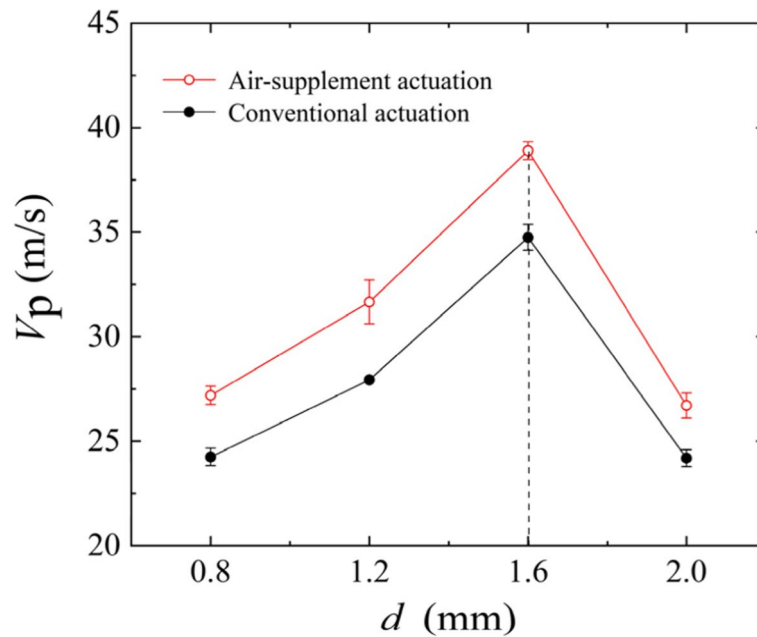


Fig. 12 Air-supplement PSJ velocities according to jet orifice diameter

4.2 Flow separation control effect comparison

Subsequently, a wind tunnel test was conducted by using a single actuator with different d , and the results are shown in Fig. 13. The experimental results show that the larger the d , the better the air-supplement PSJ flow control effect. When $d \geq 1.6$ mm, the airfoil flow separation α^* under air-supplement actuation increases by 4° and 1° , respectively, compared with that under non-actuation and $d \leq 1.2$ mm.

Under non-actuation, the flow field on the airfoil upper surface is separated at $\alpha = 8^\circ$. After separation occurs, with increasing α , the backflow region area expands, and the separation point moves forward, so the separation becomes worse. Under air-supplement actuation, flow separation is effectively suppressed. When $d = 0.8$ and 1.2 mm, α^* increases from 8° to 11° , respectively (Fig. 13e and h); hence, $\Delta\alpha^* = 3^\circ$ compared with that under non-actuation. When d increases to 1.6 and 2.0 mm, the jet flow separation control effect is further improved. At this time, $\alpha^* = 12^\circ$ (Fig. 13l and o); hence, $\Delta\alpha^* = 4^\circ$ compared with that under non-actuation.

Increasing d not only changes the jet velocity, but also the jet mass flow rate. To reflect the effect of d on the flow control more accurately, a dimensionless jet momentum coefficient C_μ [33] is defined to characterize the PSJ energy under different d , as shown in Eq. (2).

$$C_\mu = \frac{\rho_j V_a^2 h_j d}{\rho_\infty v_\infty^2 c l}, \quad (2)$$

where ρ_∞ is the incoming flow density, 1.203 kg/m^3 ; v_∞ is the incoming flow speed; c and l are the airfoil model chord length and span, respectively; ρ_j is the jet gas density,

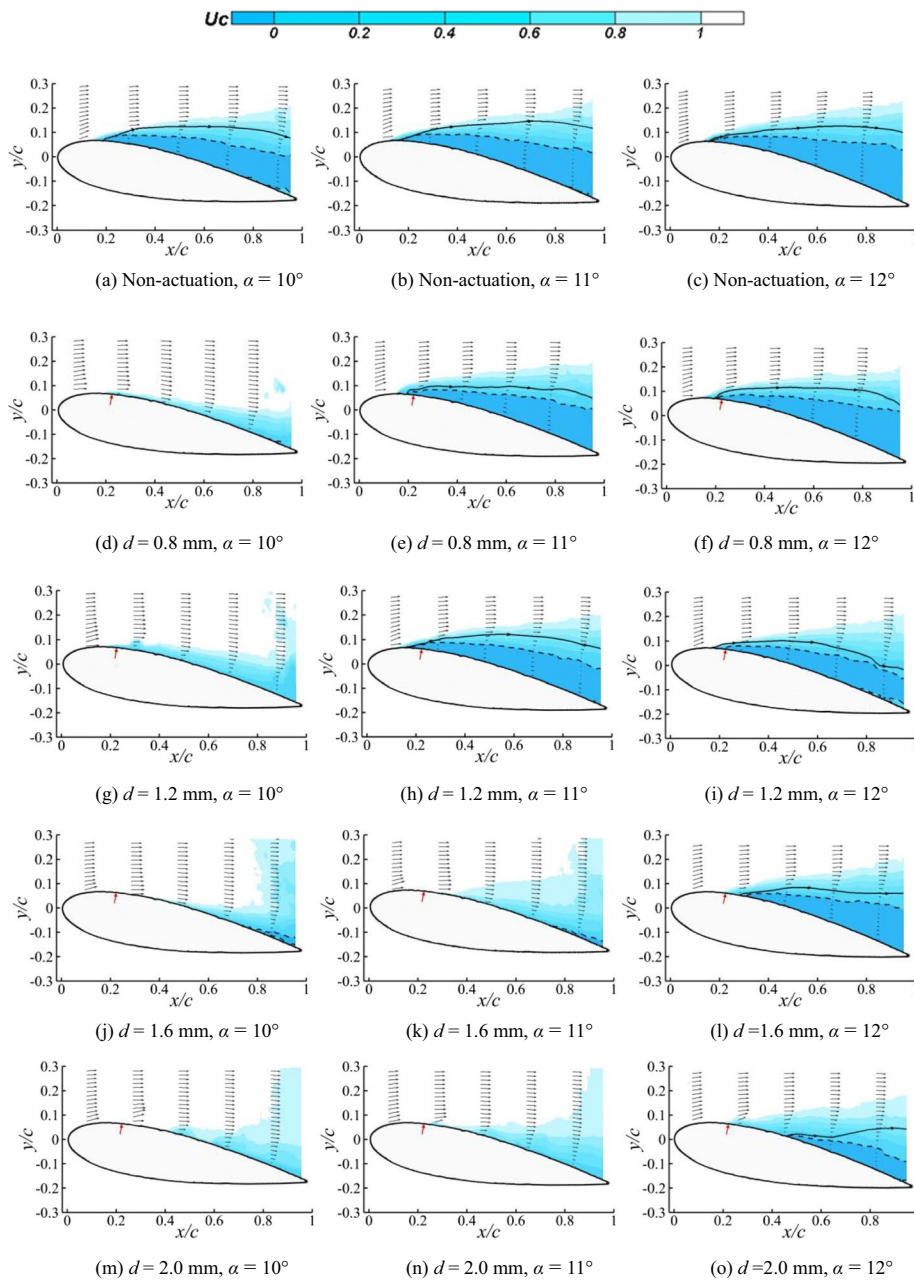


Fig. 13 Flow field velocity contours for different jet orifice diameters

approximately taking the incoming flow density ρ_{∞} ; V_a is the average jet velocity; h_j is the jet outlet throat length; and d is the jet orifice diameter.

At $\alpha = 12^\circ$, with increasing d , C_μ increases, $S_{U<0}/S_0$ decreases, and s/c is delayed (Fig. 14). When $d = 2.0$ mm, compared with the non-actuation state and $d = 0.8$ mm, the backflow region area is decreased by 68.1% and 62.2%, respectively, and the separation point position is delayed by 30.7% c and 27.0% c , respectively. Thus, the larger the d , the stronger the jet energy. PSJ has a more obvious control effect on the flow separation of the airfoil.

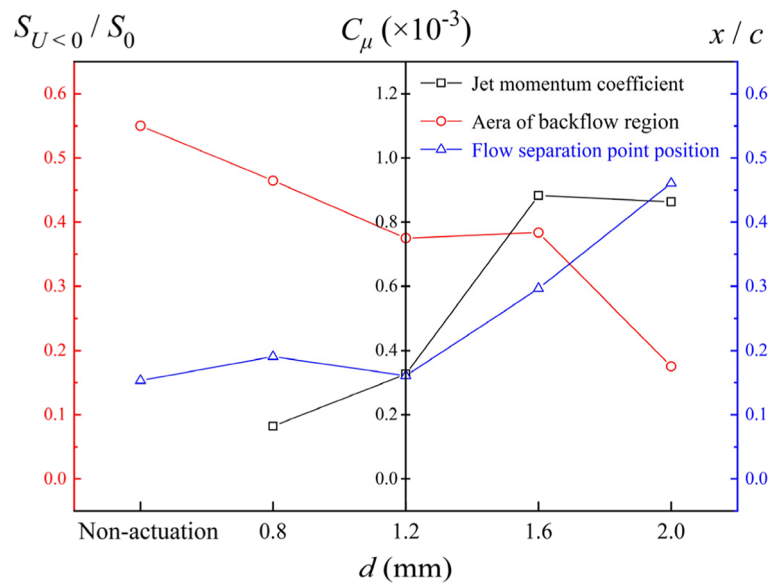


Fig. 14 Flow separation characteristic parameter and jet momentum coefficient variation according to the jet orifice diameter at $\alpha = 12^\circ$

4.3 Flow control effect comparison between the conventional and air-supplement actuation states

With increasing d , the flow control effect of the conventional excitation is also enhanced, but the enhanced control effect is still significantly weaker than that under air-supplement PSJ actuation with the same diameter (Figs. 13 and 15). On the one hand, when $d = 2.0\text{ mm}$, α^* under conventional actuation is increased by 3° compared with that under non-actuation but is still less than that under air-supplement actuation. On the other hand, when $\alpha = 12^\circ$, compared with the conventional actuation state, the separation point is delayed by $16.0\%c$ and the backflow region area is decreased by 37.9% in the air-supplement actuation state (Table 2). This finding further proves that the jet flow separation control effect under air-supplement actuation is noticeably better than that under conventional actuation.

To summarize, the flow control effect of a PSJ under air-supplement actuation is superior to that under conventional actuation and is affected by the jet orifice diameter. The larger the diameter, the better the control effect. In practical flow control applications, the jet orifice diameter should be set reasonably to obtain the best flow control effect.

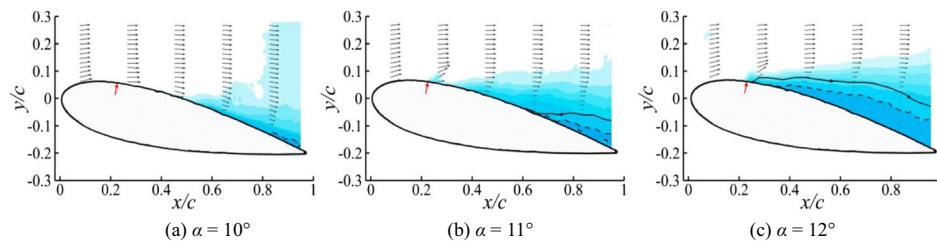


Fig. 15 Flow field velocity contours under conventional actuation for different jet orifice diameters

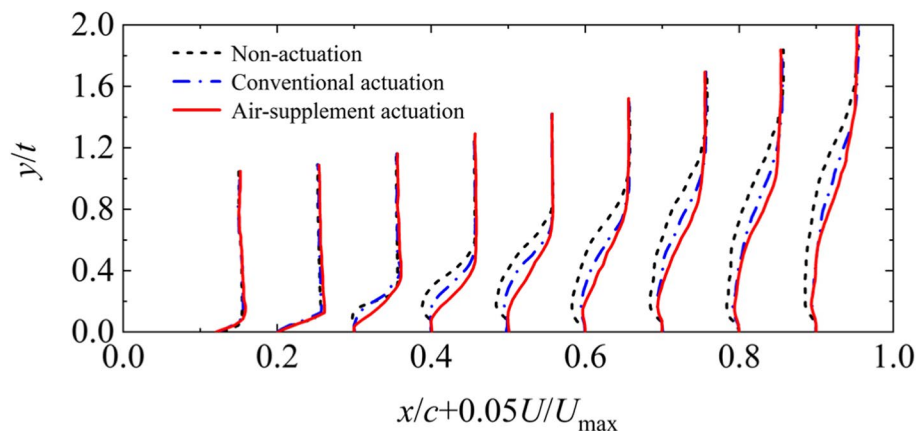
Table 2 Flow separation parameters under different actuation states

Actuation state	$S_{U<0}/S_0$	s/c
Conventional	0.29	0.30
Air-supplement	0.18	0.46

4.4 Velocity profiles and displacement thickness under different actuation states

To explore the flow separation control mechanism with the air-supplement PSJ with different jet orifices, we compared the changes in velocity profile, δ^* , and flow field vortex structure under the different actuation states based on the results at $\alpha = 12^\circ$ presented in Section 4.3 (Figs. 13c, o, and 15c). Figure 16 shows the velocity profiles of the upper wing under the three different actuation states at $\alpha = 12^\circ$.

Compared with the non-actuation and conventional actuation states, the velocity profile at each flow field position under air-supplement actuation is fuller, the flow velocity is greater at the same height, and the ability of the air flow to resist the reverse pressure gradient is stronger. Therefore, the airfoil flow separation α^* is improved (Figs. 13 and 15). Under non-actuation, the flow starts to separate in a wide range from the leading edge. Due to the viscous force at the bottom of the boundary layer and the flow field inverse pressure gradient, the airflow velocity near the wall gradually decreases. At $x/c = 0.15$, the airflow velocity decreases to zero, and flow separation starts. Under conventional actuation, the boundary layer velocity profile gradually becomes fuller, and the ability to resist the inverse pressure gradient is enhanced. The separation point is delayed to $x/c = 0.30$, and the backflow region area is decreased by 47.3% compared with that under non-actuation. Under air-supplement actuation, the boundary layer velocity profile becomes much fuller than that under conventional actuation, and the separation point is further delayed to $x/c = 0.46$. The backflow region area is greatly decreased, being 68.1% and 37.9% smaller than that under non-actuation and conventional actuation, respectively. It is sufficient to show that the PSJ in the air-supplement actuation state improves the ability of the boundary layer to resist the inverse pressure gradient more than in the conventional actuation state. In addition to qualitatively analyzing the velocity profiles, we quantitatively compared the variations in δ^* according to x/c under the three different actuation states (Fig. 17).

**Fig. 16** Velocity profiles of the suction surface under different actuation states

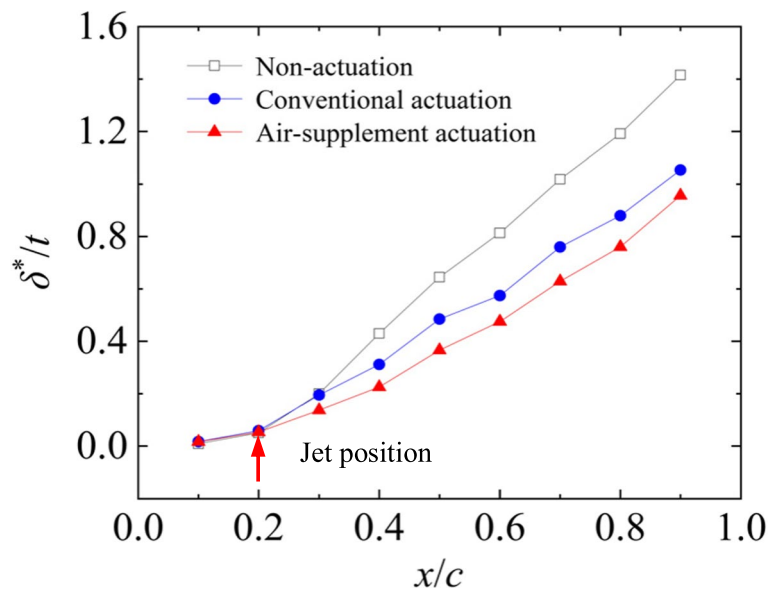


Fig. 17 Boundary layer displacement thickness under different actuation states

Compared with the non-actuation state, the jet can decrease δ^* under conventional and air-supplement actuation when $x/c > 0.2$ (the red arrow position in Fig. 17). Moreover, the control effect under air-supplement actuation is better. Overall, δ^* under air-supplement actuation is approximately 15% thinner than under conventional actuation. The smaller the δ^* , the stronger the ability of the boundary layer to resist the inverse pressure gradient, and the higher the ability to suppress the flow separation.

4.5 Vortex structure on the airfoil upper surface under different actuation states

Based on the velocity fields shown in Figs. 13a, o, and 15c, the flow field vortex contour and streamline diagram of the airfoil upper surface under the three actuation states at $\alpha = 12^\circ$ are given in Fig. 18. The vortex is identified via the Q criterion. Under non-actuation (Fig. 18a), the vortex structure is similar to that in Fig. 11a. Under conventional actuation (Fig. 18b), after the jet is sprayed, it interacts with the mainstream and generates a strong flow direction counter-vortex at the jet actuation position. At the jet actuation position, the contour-vortex is in the early developing stage and the vortex is strong and maintains a relatively complete structure. It can be observed that the actuation of two adjacent jets produces two counter-vortex pairs. The counter-vortex develops downstream from the main stream and gradually dissipates, evolving into an

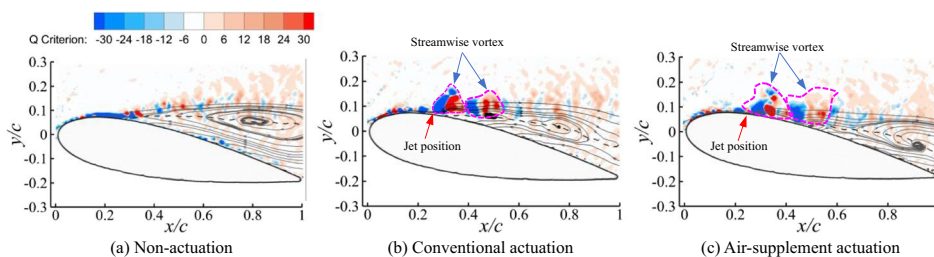


Fig. 18 Vortex contour and streamlines in different actuation states at $\alpha = 12^\circ$

irregular vortex structure. From the streamline analysis, under jet actuation, the separation point is delayed, and the backflow region and the flow separation range are greatly reduced. The separation vortex scale is reduced, showing a multi-vortex structure. It is worth noting that near the jet actuation position, the streamlines are arched by the jet and deformed. Thus, a high-speed PSJ has a strong disturbance effect on the flow field.

Under air-supplement actuation (Fig. 18c), the jet energy is higher (Fig. 12), and the action range of the generated counter-vortex is significantly larger than that under conventional actuation; additionally, the first two adjacent counter-vortex pairs are basically applied to the airfoil surface. From the streamline analysis, the separation point is delayed more and the backflow region and the flow separation range are smaller than those under conventional actuation. The separated vortex scale near the leading edge is noticeably reduced and presents a multi-vortex structure. Furthermore, near the jet actuation position, the streamlines are arched by the jet and deformed, but the deformation degree is slightly smaller than that under conventional excitation. Thus, the PSJ flow control effect under air-supplement actuation is noticeably better than that under conventional actuation.

5 Discussion on the flow control mechanism

Based on the flow field analysis results, the PSJ flow control mechanism can be described in terms of two aspects. On the one hand, there are two direct effects of energy injection during the jet ejection stage and low-energy fluid suction during the recovery stage, and these effects are stronger under air-supplement actuation. These two direct effects mainly work near the jet excitation position. Part of the jet energy accelerates the boundary layer flow and absorbs the bottom low-energy fluid to enhance the boundary layer energy. The direct energy injection requires a higher jet velocity, which is only reflected under air-supplement actuation. In Figs. 16 and 17, at $x/c=0.3$, the boundary layer velocity profile becomes fuller only under air-supplement actuation (Fig. 14), and the boundary layer displacement thickness decreases by 30%. However, the range of the direct effect is limited, and it has a secondary role.

On the other hand, the PSJ produces an indirect mixing effect due to the counter-vortex (Figs. 11 and 18), which increases the boundary layer energy, and the vortex mixing effect on the boundary layer is better under air-supplement actuation. The PSJ is a high-frequency pulsed jet. Under the action of such a jet, a periodic counter-vortex sequence is formed with the main stream gradually developing downstream (Figs. 11c and 18b, c), where the first two adjacent counter-vortex pairs have the strongest effect on the boundary layer. Under air-supplement actuation, the action range of the counter-vortex is larger than that under conventional actuation, and the boundary layer mixing effect is better. The boundary layer velocity profile is fuller (Figs. 9 and 16), the boundary layer displacement thickness is smaller (Figs. 10 and 17), and the ability to resist the inverse pressure gradient is stronger. Therefore, the jet can further delay the separation and reduce the flow separation and backflow region areas under air-supplement actuation (Figs. 13 and 14, Table 2). The indirect effect of vortex mixing works in a wider range, and it is dominant [27, 28]. In practical flow control applications, focus should be placed on enhancing the vortex mixing effect to further improve the PSJ flow control effect.

The mechanism summarized above is similar to that obtained by Zong et al. [13]. A PSJ with an appropriate actuation position and frequency can make the zero-velocity line periodically close to the airfoil upper surface through the mixing enhancement effect on the boundary layer flow, which plays a role in inhibiting flow separation.

Furthermore, the above mechanism can explain why the flow control effect is improved by increasing the jet orifice diameter. As the jet orifice diameter increases, the momentum coefficient of the jet increases (Fig. 14), which means that the jet energy increases, enhancing the injection energy and suction effect accordingly. More importantly, the intensity of the generated counter-vortex sequence also increases, and the boundary layer mixing effect is strengthened so that the boundary layer velocity profile is much fuller, the displacement thickness is smaller, and the ability to resist the inverse pressure gradient is higher, which can inhibit flow separation and improve the flow separation critical attack angle (Fig. 13).

6 Conclusion

In this study, to address the knowledge gaps in the flow control of air-supplement PSJs, we experimentally investigated their control effects, influencing factors, and mechanisms. Additionally, we proved the excellent control effect of air-supplement PSJs and clarified the jet flow separation control mechanism by comparing the critical attack angle α^* , backflow area $S_{U<0}$, separation point position s/c , velocity profile, displacement thickness δ^* , and vortex structure contour of a NACA0021 2D airfoil under different actuation states. The main conclusions of this study can be summarized as follows.

- (a) A PSJ can decrease the boundary layer thickness, the flow separation, and the backflow region; suppress flow separation; and improve the flow separation critical attack angle. Compared with the conventional actuation state, the flow control effect is better under air-supplement actuation. When $Re = 6.7 \times 10^4$, the critical attack angle α^* increases by 3° and 1° , respectively, compared with the non-actuation and conventional actuation states. At an attack angle of 12° , compared with the conventional excitation state, the jet under air-supplement actuation decreases the boundary layer thickness by 15%, delays the separation point by $16.0\%c$, and minimizes the backflow region by 37.9%.
- (b) The PSJ flow control effect is related to the momentum coefficient of the jet. In this experiment, increasing the jet orifice diameter could improve the jet momentum coefficient, enhance the flow separation suppression, and increase the flow separation critical attack angle.
- (c) The dominant mechanism through which PSJs can control flow separation is the indirect mixing effect by the counter-vortex sequence produced by the pulsed jet, which improves the boundary layer energy and enhances its ability to resist the inverse pressure gradient, thus delaying flow separation. Under air-supplement actuation, the action range of the counter-vortex is larger than that under conventional actuation, and the boundary layer mixing effect is better. PSJs can further delay flow separation, decrease the separation and backflow region areas, and improve the flow separation critical attack angle.

Despite its many advantages, this study also has some deficiencies. For example, due to wind tunnel and 2D airfoil model limitations, the number of jets arranged is limited. Subsequently, the model size needs to be adjusted to increase the number of jets. Furthermore, it is necessary to further study the influence of the control position and the jet direction on the control effect, as well as improving the counter-vortex mixing effect and the active flow control effect. Presently, the flow control Re is relatively low, so it is necessary to further study the flow control effect of the air-supplement PSJ at higher Re to improve its practical application value.

Abbreviations

PIV	Particle image velocimetry
PSJ	Plasma synthetic jet

Acknowledgements

We would like to thank Professor Xuan-Shi Meng from Northwestern Polytechnical University for his suggestion on the experimental airfoil model design.

Authors' contributions

R.-B. Liu: Analysis, Writing, Reviewing and Editing. W.-T. Wei, H.-P. Wan, and F. Li: Experiment, Writing original draft. Q. Lin: Methodology, Supervision. K. Tang: Funding acquisition. All authors read and approved the final manuscript.

Funding

This material is based on work supported by the Fundamental Research Funds for the Central Universities of China (Grant no. 20720210050); the Natural Science Foundation of China (Grant no. 51707169); the Open Fund of Rotor Aerodynamics Key Laboratory, China Aerodynamics Research and Development Center (Grant no. RAL202103-1); and the Xiamen University Training Program of Innovation and Entrepreneurship for Undergraduates (Grant no. 202110384082).

Availability of data and materials

Not applicable.

Declarations

Competing interests

The authors declare that they have no competing interests.

Received: 11 July 2022 Accepted: 13 September 2022

Published online: 23 October 2022

References

- Grossman KR, Cybyk BZ, VanWie DM (2003) Sparkjet actuators for flow control. Paper presented at the 41st aerospace sciences meeting and exhibit, Reno, 6-9 January 2003
- Cybyk BZ, Simon DH, Land HB et al (2006) Experimental characterization of a supersonic flow control actuator. Paper presented at the 44th AIAA aerospace sciences meeting and exhibit, Reno, 9-12 January 2006
- Popkin SH, Cybyk BZ, Land HB et al (2013) Recent performance-based advances in Sparkjet actuator design for supersonic flow applications. Paper presented at the 51st AIAA aerospace sciences meeting including the new horizons forum and aerospace exposition, Grapevine, 7-10 January 2013
- Popkin SH, Cybyk BZ, Foster CH et al (2016) Experimental estimation of SparkJet efficiency. *AIAA J* 54(6):1831–1845
- Zong HH (2018) Influence of nondimensional heating volume on efficiency of plasma synthetic jet actuators. *AIAA J* 56(5):2075–2078
- Zong HH, Kotsonis M (2016) Electro-mechanical efficiency of plasma synthetic jet actuator driven by capacitive discharge. *J Phys D Appl Phys* 49(45):455201
- Belinger A, Hardy P, Barricau P et al (2011) Influence of the energy dissipation rate in the discharge of a plasma synthetic jet actuator. *J Phys D Appl Phys* 44(36):365201
- Wu SQ, Liu XY, Huang GW et al (2019) Influence of high-voltage pulse parameters on the propagation of a plasma synthetic jet. *Plasma Sci Technol* 21(7):074007
- Caruana D, Barricau P, Gleyzes C (2013) Separation control with plasma synthetic jet actuators. *Int J Aerodyn* 3(1):71–83
- Liu RB, Niu ZG, Wang MM et al (2015) Aerodynamic control of NACA 0021 airfoil model with spark discharge plasma synthetic jets. *Sci China Technol Sci* 58(11):1949–1955
- Li Y, Liang H, Jia M et al (2017) Experimental investigation of enhancing wing aerodynamic performance by plasma synthetic jet. *J Propuls Technol* 38(09):1943–1949 (in Chinese)
- Su Z, Li J, Liang H et al (2018) Experimental investigation of enhancing airfoil aerodynamic performance with multi-channel plasma synthetic jet. *J Propuls Technol* 39(09):1928–1937 (in Chinese)

13. Zong HH, van Pelt T, Kotsonis M (2018) Airfoil flow separation control with plasma synthetic jets at moderate Reynolds number. *Exp Fluids* 59:169
14. Gu RY, Shan Y, Zhang JZ et al (2018) Numerical study on transport aircraft after-body flow separation control by spark jet. *J Aerospace Power* 33(8):1855–1863 (in Chinese)
15. Sun J, Niu ZG, Liu RB et al (2019) The wind tunnel test of the active flow control on the flying wing model based on the plasma synthetic jet. *J Exp Fluid Mech* 33(4):81–88 (in Chinese)
16. Zhou Y, Xia Z, Luo Z et al (2017) Effect of three-electrode plasma synthetic jet actuator on shock wave control. *Sci China Technol Sci* 60:146–152
17. Zhou Y, Xia Z, Luo Z et al (2019) Characterization of three-electrode SparkJet actuator for hypersonic flow control. *AIAA J* 57(2):879–885
18. Zhou Y, Xia ZX, Luo ZB et al (2017) A novel ram-air plasma synthetic jet actuator for near space high-speed flow control. *Acta Astronaut* 133:95–102
19. Li JF, Zhang XB (2020) Active flow control for supersonic aircraft: a novel hybrid synthetic jet actuator. *Sens Actuat A Phys* 302:111770
20. Emerick T, Ali MY, Foster C et al (2014) SparkJet characterizations in quiescent and supersonic flowfields. *Exp Fluids* 55:1858
21. Zhou Y, Xia ZX, Luo ZB et al (2019) Characterization of plasma synthetic jet actuator with cavity pressurization. *J National Univ Defense Technol* 41(6):12–18 (in Chinese)
22. Liu RB, Wang MM, Hao M et al (2016) Experimental research on air supplementing type plasma synthetic jet generator. *Acta Aeronaut Astronaut Sin* 37(6):1713–1721 (in Chinese)
23. Liu RB, Li F, Wei WT et al (2021) One-way valve and plasma synthetic jet actuator, China Patent ZL 202010788934.1, 13 July 2021
24. Liu RB, Wei WT, Li F et al (2022) Working mechanism of air-supplement plasma synthetic jet actuator. *Acta Aeronaut Astronaut Sin* 43(8):125854 (in Chinese)
25. Amitay M, Smith DR, Kibens V et al (2001) Aerodynamic flow control over an unconventional airfoil using synthetic jet actuators. *AIAA J* 39(3):361–370
26. Chen YS (2019) Performance improvements of plasma synthesis jet and application in active flow control. Dissertation, Xiamen University, Xiamen China (in Chinese)
27. Zong HH, Kotsonis M (2017) Interaction between plasma synthetic jet and subsonic turbulent boundary layer. *Phys Fluids* 29(4):045104
28. Zhao GQ, Zhao QJ, Gu YS et al (2015) Experimental investigation of synthetic jet control on large flow separation of airfoil during stall. *Chin J Theoret Appl Mech* 47(2):351–355 (in Chinese)
29. Feng HH, Liu Y, Wei ZY et al (2020) Numerical study on the effects of porous on the boundary layer of airfoil flow. *Chin J Appl Mech* 37(3):1160–1165 (in Chinese)
30. Cybyk BZ, Grossman KR, Wilkerson JT (2005) Single-pulse performance of the SparkJet flow control actuator. Paper presented at the 43rd AIAA aerospace sciences meeting and exhibit, Reno, 10–13 January 2005
31. Zong HH, Wu Y, Jia M et al (2016) Influence of geometrical parameters on performance of plasma synthetic jet actuator. *J Phys D Appl Phys* 49:025504
32. Zhou Y, Xia ZX, Luo ZB et al (2018) Experimental characteristics of a two-electrode plasma synthetic jet actuator array in serial. *Chin J Aeronaut* 31(12):2234–2247
33. He P, Dong JZ (2015) Effect of slot orientation on synthetic jet-based separation control in a serpentine inlet. *J Aerosp Power* 30(2):306–314 (in Chinese)

Publisher's Note

Springer Nature remains neutral with regard to jurisdictional claims in published maps and institutional affiliations.

Submit your manuscript to a SpringerOpen[®] journal and benefit from:

- Convenient online submission
- Rigorous peer review
- Open access: articles freely available online
- High visibility within the field
- Retaining the copyright to your article

Submit your next manuscript at ► [springeropen.com](https://www.springeropen.com)
